

# Modeling and Bending Test Simulations of Cement Treated Soil

K. Kaneda<sup>1</sup>, T. Tanikawa<sup>1</sup> and S. Onimaru<sup>1</sup>

<sup>1</sup>Takenaka Corporation, Takenaka Research & Development Institute, Chiba, Japan

E-mail: kaneda.kazuhiro@takenaka.co.jp

**ABSTRACT:** Cement treated soil, which is commonly utilized to prevent liquefaction and/or to increase the bearing capacity of soft clay foundations, is characterized by four basic properties: 1) its strength is greater than that of untreated soil, yet less than that of concrete, 2) it exhibits nonlinear behavior close to its peak strength, 3) softening occurs after its peak strength has been exceeded, and 4) the extension strength is found while the soil is not considered. In this study, the subloading surface model introduced by Hashiguchi was incorporated into a modified Drucker-Prager criterion, and undrained triaxial compression tests of cement treated soil were performed under constrained pressures of 0.1 and 0.4 MN/m<sup>2</sup>, after which bending tests and simulations were performed. The numerical results of these tests agreed well with the actual results of element wise and boundary condition testing.

## 1. INTRODUCTION

Recently, increasing numbers of construction projects are being erected on soft clay and medium loose sand. In the case of soft clay, settlement stability or load bearing capacity is the most relevant concern, while the potential for liquefaction is the most important consideration in the case of medium loose sand. Among the various soil improvement methods is the deep mixing method, in which soil is strengthened by mixing it with cement. Thus, there are now numerous examples of construction sites where cement treated soil has been used (Saito, *et al.*, 1996, Yu, *et al.*, 1998, Lee, *et al.*, 2004, Koseki, *et al.*, 2005, Namikawa and Koseki, 2006, Horpibulsuk, *et al.*, 2010, Suebsuk, *et al.*, 2010).

The four typical features of cement treated soils are as follows (Kaneda, *et al.*, 2012)

- 1) Its strength is greater than that of conventional soil, yet less than that of concrete.
- 2) It exhibits nonlinear behavior close to its peak strength.
- 3) Softening occurs after the peak strength has been surpassed.
- 4) The extension strength is found while the soil is not considered.

Although the strength of cement treated soil is relatively high, in Japan, the method has been used primarily to provide foundations for temporary structures because such soil lacks the strength that can be obtained via steel or concrete pilings. However, cement treated soil is gaining increased attention for use in the foundations of permanent structures because it provides greater strength than untreated soils, and is more economical than steel or concrete pilings (Yamashita, *et al.*, 2011, Uchida, *et al.*, 2012).

This increased attention has stimulated demands for cement treated soil types with greater bearing capacity, which will be needed to support the tall and / or heavy structures envisioned for construction, along with demands for more detailed information on the earthquake resistance of such soil types. These expected demands have thus highlighted the need for a constitutive model for cement treated soil.

Previous investigations into cement treated soil have focused on methods of applying the constitutive equations for concrete, applying the Mohr-Coulomb criteria to failure energy (Namikawa and Koseki, 2007), and applying the Cam-clay model to consider extension strength (Hashiguchi and Mase, 2007). Furthermore, softening has not previously been considered in the approach based on the constitutive equations for concrete, and there are difficulties in determining the parameters in the approach based on the Cam-clay model.

This aim of this study is to create new simplified constitutive equations for cement treated soil that contain fewer parameters. To accomplish this, undrained triaxial compression tests were performed on cement treated soil under constrained pressures of 0.1 and 0.4 MN/m<sup>2</sup>, after which bending tests were conducted as a boundary condition problem to investigate the performance of the model.

## 2. CEMENT TREATED SOIL MODELING

This new model is based on a modified Drucker-Prager criterion and is combined with the subloading yield concept.

### 2.1 Normal-yield function

The modified Drucker-Prager criterion, introduced by Tanabe *et al.*, 1994, was developed as a constitutive equation for concrete (Chen, 1982). While the Drucker-Prager criterion is very simple, the yield curve shape is not smooth at  $J_2=0$ , and the extension strength is overestimated. The modification introduced by Tanabe *et al.* (shown in the equations below) results in a smoothed yield curve shape at  $J_2=0$ , and at high compression stress, this model approaches the original Drucker-Prager yield surface.

$$F(\sigma, k) = J_2 - (k_f - \alpha_f I_1)^2 + (k_f - \alpha_f \eta)^2 = 0 \quad (1)$$

$$k_f = \frac{6c \cos \phi}{\sqrt{3}(3 + y \sin \phi_1)} \quad (2)$$

$$\alpha_f = \frac{2 \sin \phi}{\sqrt{3}(3 + y \sin \phi_1)} \quad (3)$$

where  $I_1 = \sigma_{ii}$  and  $J_2 = \frac{1}{2} S_{ij} S_{ij}$

are the first invariant and second deviator invariant of the stress tensor, respectively,  $c$  is the cohesion,  $\phi$  is the friction angle,  $y$  is a variable determining the yield shape, and  $\phi_1$  and  $\eta$  are material constants. In this study, it is assumed that  $y=-1$  (Compression strength at Mohr-Coulomb criterion) and  $\phi_1 = \phi$ . The material constant  $\eta$  is related to the extension strength.

### 2.2 Subloading yield function

The subloading yield surface was introduced by Hashiguchi (Hashiguchi, 1989), and is shown in Figure 1. This surface is inside of the normal-yield surface, and the center of similarity is origin.  $R(0 \leq R \leq 1)$  is the ratio of the normal-yield surface to the subloading yield surface. The subloading yield surface is determined via the following equations:

$$\bar{F}(\sigma, k) = J_2 - (Rk_f - \alpha_f I_1)^2 + (Rk_f - \alpha_f \eta)^2 = 0 \quad (4)$$

$$R(0 < R \leq 1) \quad (5)$$

When  $R$  approaches 0, strong elastic behavior is exhibited. In contrast, when  $R$  reaches 1, the subloading yield surface coincides with the normal-yield surface.  $R_0$ , which is the "elastic limit", is then introduced. When  $R$  is less than  $R_0$ , pure elastic behavior is indicated.

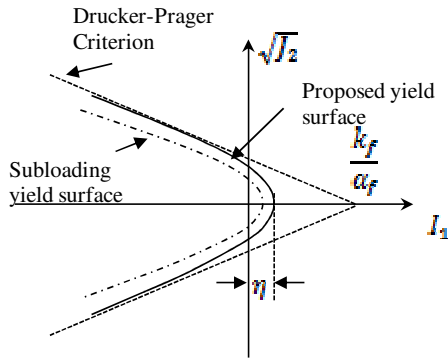


Figure 1 Two yield surfaces

**2.3 Compatibility condition and flow rule**

The time differentiation of equation (4) is satisfied using Prager's compatibility condition, as seen below:

$$\frac{\partial \bar{F}(\sigma, k)}{\partial \sigma} \cdot \dot{\sigma} + \frac{\partial \bar{F}(\sigma, k)}{\partial R} \cdot \dot{R} + \frac{\partial \bar{F}(\sigma, k)}{\partial k} \frac{\partial k}{\partial \kappa} \cdot d\kappa = 0 \tag{6}$$

The associate flow rule is then assumed.

$$\dot{\epsilon}^p = \lambda \frac{\partial \bar{F}(\sigma, k)}{\partial \sigma} \tag{7}$$

where,  $F$  is the plastic potential,  $\lambda$  is the plastic multiplier and  $\dot{\epsilon}^p$  is the plastic strain rate.

**2.4 Evolution law**

The evolution law for  $R$  are given as follows:

When  $\dot{\epsilon}^p \neq 0, \dot{R} > 0$

When  $\dot{R} > 0, \dot{\epsilon}^p \neq 0$  (8)

When  $\dot{\epsilon}^p = 0, \dot{R} = 0$

$$\dot{R} = U \|\dot{\epsilon}^p\| \tag{9}$$

where,  $U$  is a positive function when  $(0 \leq R \leq 1)$ , as shown in Figure 2.

The function  $U$  is given by:

$$U = -m \ln R \text{ when } R > R_0 \tag{10}$$

$R_0$  is the elastic limit. When  $R_0 > R$ , pure elastic behavior is exhibit.

The subloading coefficient  $m$  is a material constant, which can be determined from experimental results.  $m$  is the rate of approach to the normal-yield surface under plastic deformation. When  $m$  is extremely large, strong elastic behavior is exhibited until the subloading yield surface reaches the normal-yield surface. In contrast, when  $m$  is small, nonlinearity occurs at the beginning of deformation.

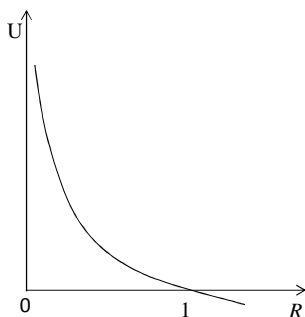


Figure 2 Function U

**2.5 Plastic multiplier**

When equations (7) and (9) are substituted into equation (6), the plastic multiplier  $\lambda$  is given by:

$$\lambda = \frac{\frac{\partial \bar{F}(\sigma, k)}{\partial \sigma} \cdot \dot{\sigma}}{-\left( \frac{\partial \bar{F}(\sigma, k)}{\partial R} U + \frac{\partial \bar{F}(\sigma, k)}{\partial k} \frac{\partial k}{\partial \kappa} \right) \left\| \frac{\partial \bar{F}(\sigma, k)}{\partial \sigma} \right\|} \tag{11}$$

**2.6 Elasto-plastic constitutive equation**

The following decomposition of strain is assumed:

$$\epsilon = \epsilon^e + \epsilon^p \tag{12}$$

The elastic response is

$$\dot{\sigma} = E \dot{\epsilon} \tag{13}$$

Equation (13) is then substituted into equation (11).

$$\Lambda = \frac{\frac{\partial \bar{F}(\sigma, k)}{\partial \sigma} \cdot E \dot{\epsilon}}{-\left( \frac{\partial \bar{F}(\sigma, k)}{\partial R} U + \frac{\partial \bar{F}(\sigma, k)}{\partial k} \frac{\partial k}{\partial \kappa} \right) \left\| \frac{\partial \bar{F}(\sigma, k)}{\partial \sigma} \right\| + \frac{\partial \bar{F}(\sigma, k)}{\partial \sigma} \cdot E \frac{\partial \bar{F}(\sigma, k)}{\partial \sigma}} \tag{14}$$

where,  $E$  is the elastic stiffness tenor, and  $\epsilon^e$  and  $\epsilon^p$  are the elastic and plastic strain, respectively.

Finally, the elasto-plastic constitutive equation is written as follows:

$$\dot{\sigma} = E \dot{\epsilon} - \Lambda E \frac{\partial \bar{F}(\sigma, k)}{\partial \sigma} \tag{15}$$

**2.7 Loading criterion**

The loading criterion

$$\Lambda (= \lambda) > 0 \tag{16}$$

effectively guarantees that the numerator of equation (14) is also positive. Thus, the loading criterion can be given as:

$\Lambda > 0$ : loading

$\Lambda < 0$ : unloading (17)

**2.8 Softening/hardening parameter**

The softening/hardening parameter  $k(\kappa)$  is given as follows:

$$k(\kappa) = c + a \kappa \tag{18}$$

$$\kappa = \int \dot{\epsilon}^p \cdot \sigma dt \tag{19}$$

where,  $a$  is a material constant and  $c$  is the cohesion. When  $a$  is positive, hardening is indicated. In contrast, when  $a$  is negative, softening is indicated. When  $a$  is larger, the larger softening behaviour is exhibited after peak. The range of  $k(\kappa)$  is determined by the parameter  $b$ . For example,  $b$  is presented by the residual stress when  $a$  is negative.

$$k(\kappa) \leq b : a \text{ is positive}$$

$$k(\kappa) \geq b : a \text{ is negative} \tag{20}$$

After the peak, the load declines, and the structure is considered to become unstable due to the development of a shear band. In this study, it is considered that softening results from the properties of

the material itself. Furthermore, when softening is taken into consideration, a dependence on the analysis mesh occurs. These issues will be addressed in future studies.

### 3. CEMENT TREATED SOIL EXPERIMENTS AND SIMULATIONS

#### 3.1 Test soil production

Cement treated soil was made by mixing marine deposit clay with blast furnace cement B in the laboratory. Figure 3 shows the grain size distribution, while Table 1 shows the results of physical tests conducted on the marine deposit clay. This is clarified to be sandy clay with a high degree of liquidity. The total sand content is approximately 6.7%. Cement content was added at 300 and 400 kg/m<sup>3</sup> using a 60 and 70% water-cement ratio, respectively, which was expected to produce relatively high-strength specimens. For these experiments, cylindrical specimens with a diameter of 5 cm and a height of 10 cm were cast and then cured under constant temperature and humidity conditions for 7 or 28 days.

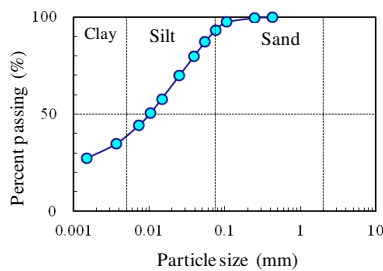


Figure 3 Grain size distribution of marine deposit clay

Table 1 Physical and chemical properties of marine deposit clay

<b>Density of soil particle</b>	$\rho_t$	g/cm <sup>3</sup>	2.620
<b>Natural water content</b>	$w$	%	129.3
<b>Consistency</b>			
<b>Liquid limit</b>	$w_L$	%	94.9
<b>Plastic limit</b>	$w_P$	%	29.9
<b>Plasticity index</b>	$I_P$		65.0
<b>pH of soils</b>			7.9

#### 3.2 The unconfined compression tests

Unconfined compression testing was performed on cylindrical specimens with a diameter of 3.5 cm and a height of 7.0 cm that had been cured for seven days. Two specimen types were produced, one with a cement content of 300 kg/m<sup>3</sup> and another with a content of 400 kg/m<sup>3</sup>, which were labeled low- and high-strength specimens, respectively. The rate of loading was set at 0.01%/min.

Table 2 shows the test results while Figure 4 shows the relationship between stress and strain. Strain was measured using an external displacement gauge. The unconfined compression strength of the low-strength sample was 3.02 and 3.16 MN/m<sup>2</sup>, the average of these two results was 3.09 MN/m<sup>2</sup>. The unconfined compression strength of the high-strength sample was 3.52~3.86 MN/m<sup>2</sup>, which resulted in an average of 3.71 MN/m<sup>2</sup>.

It is considered that extending the curing period from 7 to 28 days would result in a strength increase of 1.2~1.7. Therefore, the strength of specimens after 28 days of curing was assumed to be 3.52~3.86 and 3.71~5.25 MN/m<sup>2</sup> for low- and high-strength specimens, respectively.

In general, the design strength of cement treated soil by the grid shape soil improvement for the liquefaction is 2.0 MN/m<sup>2</sup> in Japan. Relatively high-strength cement treated soil was used in this study.

Table 2 Results of unconfined compression test

Specimen No.	300-1	300-2	400-1	400-2	400-3	400-4
Cement content	300		400			
Water content $w$	91.1	91.1	84.1	87.0	85.9	85.5
Unconfined compressive strength $q_u$	3.02	3.16	3.69	3.52	3.86	3.78
(Average value)	(3.09)			(3.71)		
Failure strain $\epsilon_f$	1.14	1.50	0.86	1.55	1.29	1.29
Modulus of deformation $E_{50}$	548	508	617	506	741	646
Mark at the peak	●	○	▲	△	■	□

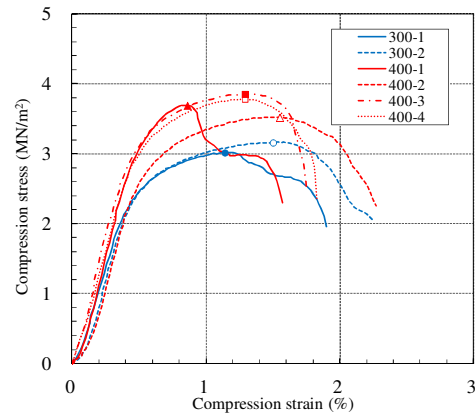


Figure 4 Relationship between stress and strain

#### 3.3 Results of undrained triaxial compression tests and simulations

Undrained triaxial compression tests of low- and high-strength specimens were performed at confining pressures of 0.1 and 0.4 MN/m<sup>2</sup>, a 0.01%/min loading rate, and under constant cell pressure conditions. In this test phase, cylindrical specimens with a diameter of 5.0 cm and a height of 10 cm that had been cured for 28 days were utilized. The strain was measured by LDT (Local displacement transducer, Goto, *et al.*, 1991) on the side of the sample.

Simulations were then performed using the new constitutive equations for cement treated soil. Table 3 shows the simulation parameters while Figure 5 shows the results of both the experiments and the simulations. The figure is divided into four sections: (a) the relationship between deviator stress and strain, (b) the relationship between deviator stress and mean effective stress, (c) the relationship between  $R$  (the ratio between the normal-yield surface and the subloading yield surface) and strain, and (d) the relationship between excess pore water pressure and strain in the experiments. The simulations were performed while paying strict attention to the nonlinearity up to the peak and to the peak strength. Those parameters were determined by the undrained triaxial and/or the unconfined compression tests. The extension strength  $T_f$  assumed to be almost 10% of compression strength.

Table 3 Material constants

	Low-strength specimen		High-strength specimen	
	0.1	0.4	0.1	0.4
Constraint pressure (MN/m <sup>2</sup> )	0.1	0.4	0.1	0.4
Young Modulus $E$ (MN/m <sup>2</sup> )	3000		3000	
Poisson's ratio $\nu$	0.167		0.167	
Cohesion $c$ (kN/m <sup>2</sup> )	3000	3400	6600	7500
Extension strength $T_f$ (kN/m <sup>2</sup> )	500		500	
Friction angle $\phi$ (°)	20		20	
Coefficient of subloading yield surface $m$	500		1000	
Coefficient of Softening $a$	20		20	
Coefficient of Softening $b$ (kN/m <sup>2</sup> )	1000		1000	
Elastic limit $R_0$	0.01		0.01	

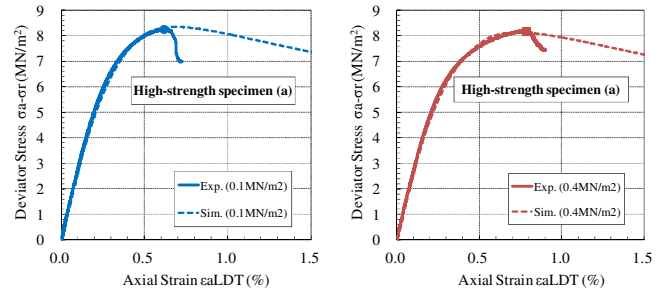
The Poisson's ratio is almost between 0.1 and 0.2 from the retrospective research (Namikawa and Koseki, 2006). Therefore the Young's modulus were determined from the initial incline of the relationship between the stress and strain, while the  $c$  (coefficient) and  $\phi$  (friction angle) were determined from the peak strength. The coefficient for the subloading yield surface and softening parameter were determined from the nonlinear region near the peak. The relationship between stress and strain is assumed to be linear, based on the linear elastic body used in the modified Drucker-Prager model and the assumption that elasticity exists inside the normal-yield surface. However, if the subloading yield concept is used, it can express the nonlinearity up to the peak.

Figure 5-(a) and 5-(b) show the experimental and simulation data for the low- and high-strength specimens. Care was taken to ensure that the initial stiffness, nonlinearity up to the peak, and softening after the peak were reproduced. In this study, the softening level after the peak was set to be gentle.

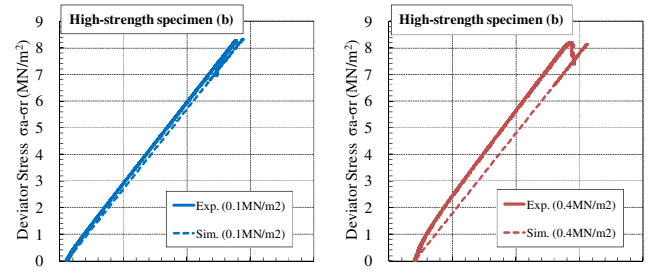
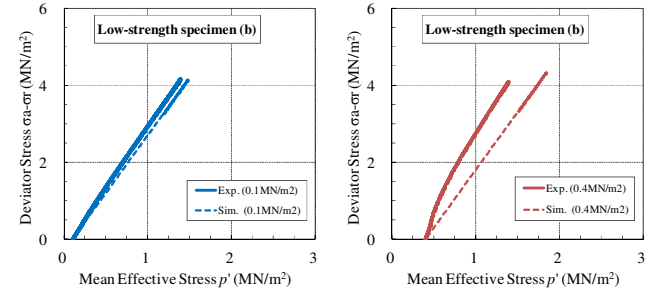
Note that, in the case of  $0.4 \text{ MN/m}^2$ , it was not possible to create a suitable simulation for the initial stage of the relationship between the deviator stress and mean effective stress.

In Figure 5-(c), it can be seen that  $R$  approaches 1 as the deformation increases, and is almost 1 for an axial strain of 1.0 %, at which point the subloading yield surface coincides with the normal-yield surface. In Figure 5-(d), it can be seen that, in the case of low-strength samples, excess pore water pressure is positive for both confining pressures. In contrast, in the case of the high-strength samples, the value is initially positive and becomes negative after 0.5% axial strain. This behavior is similar to that for over consolidated clay or dense sand. Although attempts were made to saturate specimens prior to testing, the results were inadequate. Determining an efficient method for saturating cement treated soil is another task that will be addressed in future studies. As mentioned above, since the excess pore water is not measured well in the experiment, the dilatancy of the soil may not be expressed. This task will be addressed in future studies that will take into consideration the non-associated flow rule and other factors in order to express the dilatancy of this soil.

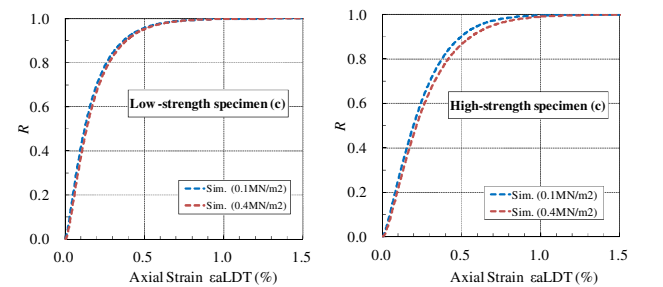
Figure 6 shows the relationship between the deviator stress and the strain assumed during the simulated unconfined extension test. The material parameters were selected for the low-strength  $0.1 \text{ MN/m}^2$  specimen shown in Table 1. The confining pressure in this simulation was set to  $0 \text{ MN/m}^2$ , as was assumed during extension test under the plain strain condition. Note that this is a simulated response, not a comparison between the experiment and simulation. Two cases were examined, one in which softening could not occur (Case 1), and another in which softening was possible (Case 2). The extension strength was  $0.45 \text{ MN/m}^2$ . Therefore,  $0.5 \text{ MN/m}^2$  was set as the parameter due to the plain strain condition. After the peak, softening behavior could be seen.



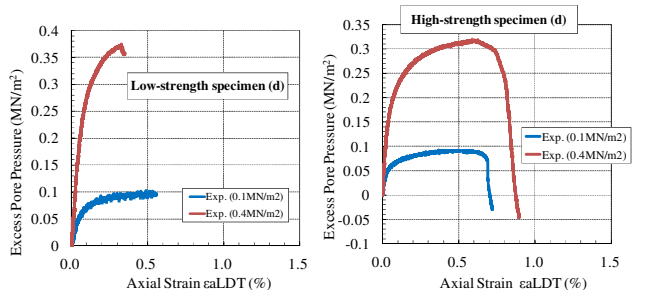
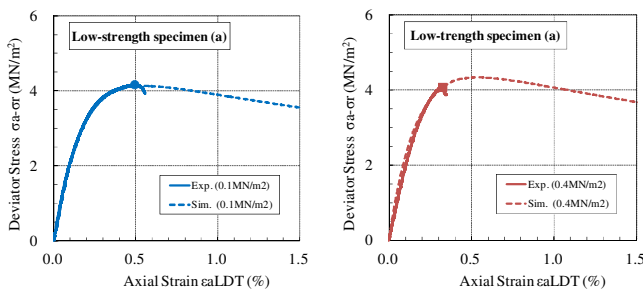
(a) Relationship between deviator stress and strain



(b) Relationship between deviator stress and mean effective stress



(c) Relationship between  $R$  (the ratio between normal-yield surface and subloading yield surface) and strain



(d) Relationship between excess pore water pressure and strain in experiments

Figure 5 Comparison between experiment and simulation

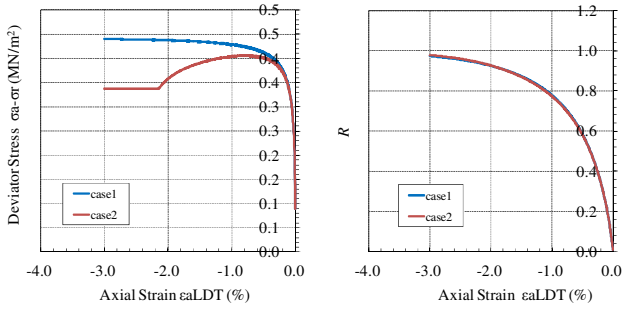


Figure 6 Relationship between deviator stress and strain assumed during the simulated unconfined extension test

4. BENDING TEST SIMULATION

4.1 Calculation conditions

This section focuses on the ability of the model to respond to the boundary value problems. Therefore, it must be emphasized that the results shown do not indicate comparisons between experimental and simulated results. Figure 7 shows the calculation mesh with the boundary conditions. The plain strain condition is assumed at one phase, a width is 12cm and a height is 4.0cm for a specimen. Both sides of the bottom were fixed in the x and y directions. The center element of length at the top was deformed to the -y direction at constant rate.

The load was calculated as the summation of the equivalent nodal forces at the deforming nodes. The black elements in Figure 7 are set to be elastic in order to prevent stress concentrations from occurring around them. Table 4 shows the material constants. The confining pressure was set to 0 MN/m<sup>2</sup>. There are two simulated cases. Case 1 is the basic case used in this study, while Case 2 is an imperfect case, in which the one underside element is truncated, as shown in Figure 7. The subject of the investigation is the development of shear strain and extension strength. Extension strength is calculated via the following equation:

$$T_j = \frac{3 Pl}{2 bD^2} \tag{21}$$

where,  $l=0.12$  m (width),  $b=1.0$  m (unit length),  $D=0.04$  m (height) and  $P$  is the force on the loading point. The Mudian program code developed by Takenaka Corporation was used in these calculations. (Shiomi, *et al.* 1993)

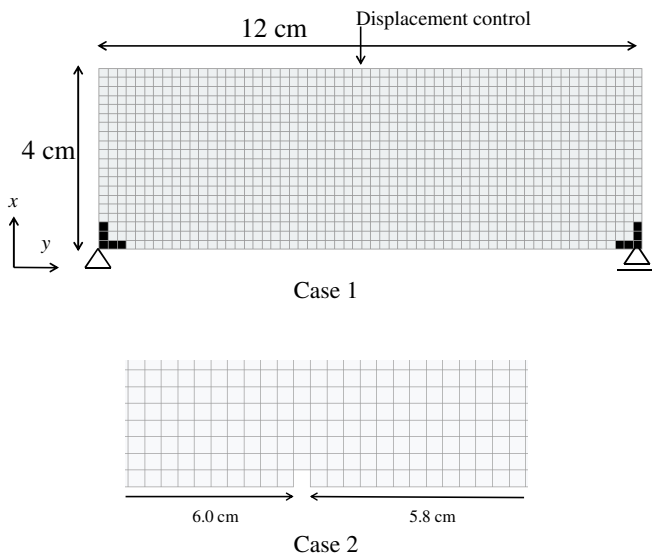


Figure 7 Calculation mesh with boundary conditions

Table 4 Material constants

Constraint pressure (MN/m <sup>2</sup> )	0
Young Modulus $E$ (MN/m <sup>2</sup> )	3000
Poisson's ratio $\nu$	0.167
Cohesion $c$ (kN/m <sup>2</sup> )	2000
Extension strength $T_f$ (kN.m <sup>2</sup> )	500
Friction angle $\phi$ (°)	20
Coefficient of subloading yield surface $m$	30
Coefficient of Softening $a$	10
Coefficient of Softening $b$ (kN/m <sup>2</sup> )	1000
Elastic limit $R_0$	0.01

4.2 Simulation results

Figure 8 shows the relationship between stress and strain observed in the simulation. In Case 1, no peak exists in spite of the nonlinearity. In Case 2, a peak is seen to exist. The peak strength (about 0.6 MPa) in Case 2 is slightly larger than the input extension strength (0.5 MPa). Figure 9 shows distributions of  $\epsilon_x$  and  $\sigma_m$  (positive range only: extension) and  $(3J_2)^{0.5}$  in the final step for each case. In all cases, the extension occurs around the base of the specimen and the strain increases from the middle. The width of the extension area spread is particularly large in Case 1.

In general, in the experiment, a number of cracks were noted around the middle section. If the specimen was perfectly homogeneous and rectangular in shape, the crack should have occurred precisely in the middle. However, imperfections will always exist in actual specimens, which are neither geometrically rectangular nor homogeneous in terms of strength, so cracks can occur in a variety of locations. This is known as the bifurcation problem.

In this study, in order to generate cracks or strain, it was necessary to introduce imperfections, such as in Case 2, where localized strain occurred from the bottom center, and was considered to have caused extension failure. On the other hand, it was noted that significant amounts of shear stress  $(3J_2)^{0.5}$  were generated as deformation progressed under the load point. This was noteworthy because the original purpose of the bending test was to investigate extension strength, and there were no plans to consider shear stress. However, in this simulation, it was found that shear stress occurred due to stress concentration at the loading point, thus indicating that both shear and extension failure would need to be considered in the boundary value problem defined by Namikawa and Koseki (2007). Therefore, it is considered necessary that the peak strength in the simulation be set slightly higher than the input extension strength. Finally, when considering the bifurcation problem, geometrical nonlinearity is important. In this research, an infinitesimal deformation was assumed. Determining ways to expand this to large deformations will be another topic of future work.

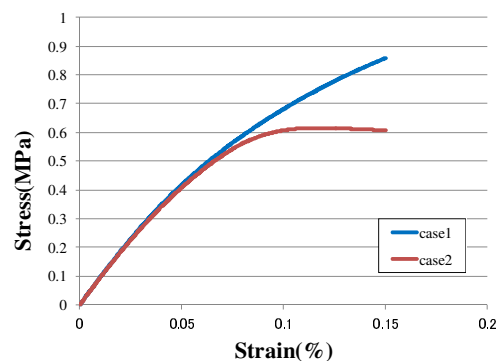


Figure 8 Relationship between stress and strain

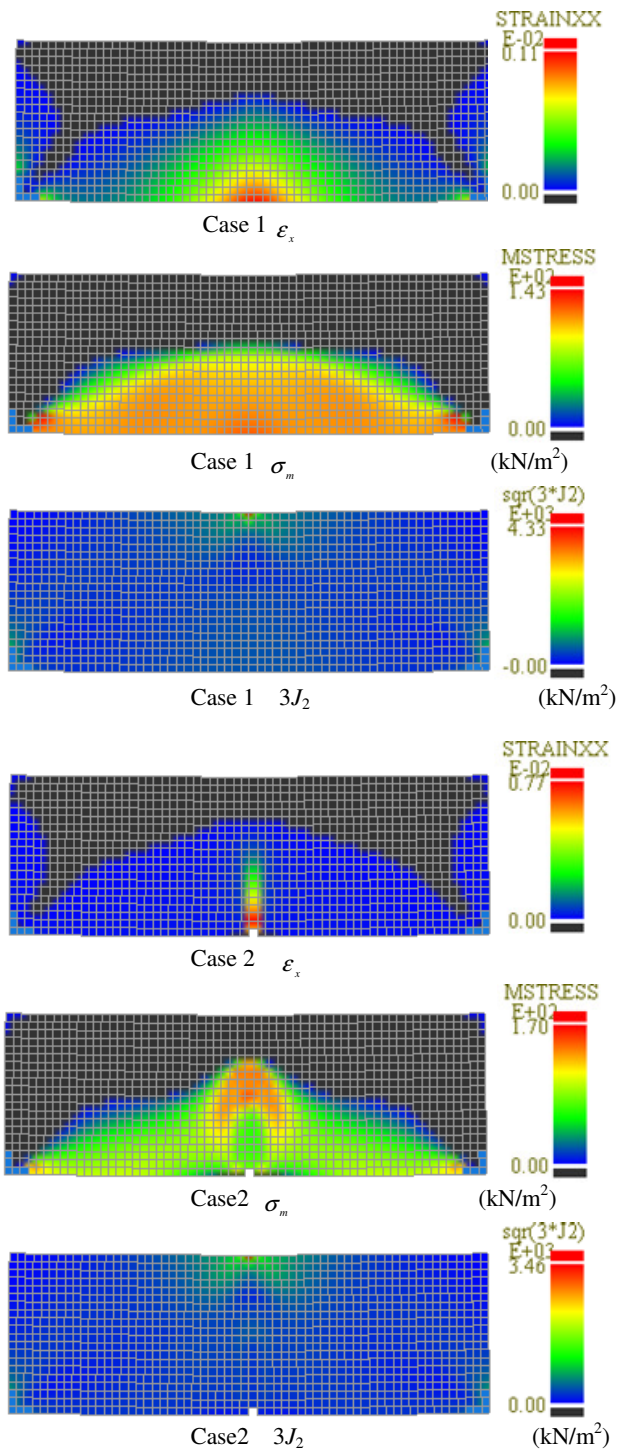


Figure 9 Distributions of  $\epsilon_x$  and  $\sigma_m$  (positive range only: extension) and  $(3J_2)^{0.5}$

## 5. CONCLUSIONS

A new constitutive cement treated soil model was developed and examined via undrained triaxial compression and bending tests. The following results were obtained:

- 1) Undrained triaxial compression tests were performed using this model and the results agreed well with those of experiments in terms of the peak strength and softening. Although attempts were made to saturate specimens prior to testing, the results were inadequate. Determining an efficient method for saturating cement treated soil is another task that will be addressed in future studies.
- 2) A bending test was performed as a boundary value problem. The extension strength of the bending test is similar to the input

extension strength. It was found that the extension strength from the boundary value problem (bending test) reproduced the value of the material inherent extension strength. Originally, it was considered desirable that there was no effect of the shear stress through the test process because the bending test is a test to investigate the extension strength. However, in this simulation, shear stress resulted from the stress concentration at the loading point, which indicated that the bending test resulted in both shear and extension failures in view of the boundary value problem.

## 6. REFERENCES

- Chen, W.F. (1982) "Plasticity in reinforced concrete", McGraw-Hill, New York.
- Goto, S., Tatsuoka, F., Shibuya, S., Kim, Y.S. and Sato, T. (1991) "A simple gauge for local small strain measurements in the laboratory", *Soils and Foundations*, Vol.31, No.1, pp 169-180.
- Hashiguchi, K. and Mase, T. (2007) "Extended yield condition of soils with tensile yield strength and rotational hardening", *Int. J. Plasticity*, Vol.13, No.12, pp 1939-1956.
- Hashiguchi, K. (1989) "Subloading surface model in unconventional plasticity", *Int. J. Solids and Structures*, 25, pp 917-945.
- Horpibulsuk, S., Liu, M.D., Liyanapathirana, D.S., and Suebsuk, J. (2010), "Behaviour of cemented clay simulated via the theoretical framework of the SCC model", *Computers and Geotechnics*, Vol.37, No.1-2, pp 1-9.
- Kaneda, K., Onimaru, S., Shigeno, Y. and Tuchiya, T. (2012) "Constitutive equation of cement treated soils and the numerical simulation of splitting test", *J. Struct. Constr. Eng., AIJ*, Vol.77, No.675, pp 723-730 (in Japanese).
- Koseki, J., Sato, T., Mihara, S., Takeya, N., and Yoshizawa, M. (2005) "Comparison of tensile strength of cement treated sand by various test method", *Deep Mixing 05*, pp 98-100.
- Lee, K., Chan, D. and Lam, K. (2004) "Constitutive model for cement treated clay in a critical state frame work", *Soils and Foundations*, Vol.44, No.3, pp 69-77.
- Namikawa, T. and Koseki, J. (2006) "Experimental determination of softening relations for cement treated sand", *Soils and Foundations*, Vol.46, No.4, pp 491-504.
- Namikawa, T. and Koseki, J. (2007) "Evaluation of tensile strength of cement-treated sand based on several types of laboratory tests", *Soils and Foundations*, Vol.47, No.4, pp657-674.
- Saito, S, Suzuki, Y., Nishioka, S. and Okumura, R. (1996) "Required strength of cement improved ground", *Grouting and Deep mixing*, Balkema, pp 557-562.
- Shiomi, T., Shigeno, Y. and Zienkiewicz, O.C. (1993) "Numerical prediction for model No. 1", *Verification of Numerical Procedures for the Analysis of Soil Liquefaction Problems* (eds. By Arulanandan and Scott), Balkema, pp 213-219.
- Suebsuk, J., Horpibulsuk, S., and Liu, M.D. (2010) "Modified Structured Cam Clay model: A Generalized Critical State Model for Destructured, Naturally Structured and Artificially Structured Clays", *Computers and Geotechnics*, Vol.37, No.7-8, pp 956-968.
- Tanabe, T., Zhishen, W.U. and Guoxiong, Y.U. (1994) "A unified plastic model for concrete", *Proc. JSCE*, No.496/V-24, pp 21-29 (in Japanese).
- Uchida, A., Yamashita, K. and Odajima, N. (2012) "Performance of Piled Raft Foundation with Grid-Form Ground Improvement During the 2011 off the Pacific Coast of Tohoku Earthquake", *Journal of Disaster Research*, Vol.7, No.6, pp 726-732.
- Yamashita, K., Hamada, J. and Yamada, T. (2011) "Field measurements on piled rafts with grid-form deep mixing walls on soft ground", *Geotechnical Engineering Journal of the SEAGS & AGSSEA*, Vol.42, No.2, pp 1-10.
- Yu, Y.Z., Pu, J.L. and Ugai, K. (1998) "A damage model for soil-cement mixture", *Soils and Foundations*, Vol.38, No.3, pp 1-12.